(Received 18 February 2025, Accepted 18 April 2025, Scheduled 28 April 2025)

A New Method for Determining Antenna Gain via Transmission Line Based Near Field Measurements in a Waveguide

Daniel Richardson, James Dee, Jonathan Yaeger, Jeramy Marsh, and Ryan S. Westafer*

Georgia Tech Research Institute, Atlanta, GA 30332, USA

ABSTRACT: Antenna gain is an important metric for most modern communication systems. The most common method for determining antenna gain is to produce an incident plane wave using a reference antenna and measure the received power at the antenna of interest. By measuring the received power several wavelengths away in an isolated environment, such as an anechoic chamber, the gain of an electrically small antenna, dimension less than one wavelength, can be determined. This and other similar methods work well for frequencies above 2 GHz, but lower frequency measurements can be logistically challenging and expensive due to the large facilities required and the lack of readily available broadband absorber materials. This work presents a new method for determining antenna gain using a transmission-line-based near-field S-parameter measurement in a waveguide. To provide evidence for the proposed method, two monopole antennas are modeled over an infinite ground plane using full-wave electromagnetics, and both are experimentally measured within a waveguide. Good agreement was found between the model and measurement, providing evidence of the validity of the method.

1. INTRODUCTION

Antenna gain is an important metric for most modern communication systems because it directly determines the fraction of power an antenna transmits or receives in a given direction, relative to isotropic. It can be determined in several ways, but the most common method is to produce an incident plane wave using a known reference antenna and measure the power received at the antenna of interest, or vice versa [1–7]. By measuring the received power several wavelengths away in an isolated environment, such as an anechoic chamber, the antenna gain can be determined. These methods often utilize the Friis equation to calculate the antenna gain from these power measurements. This method and other similar methods work well for frequencies above approximately 2 GHz, but lower-frequency measurements can be logistically challenging and expensive. An anechoic chamber at these low frequencies requires a large and expensive facility to produce reflection-free zones that imitate an isolated, free space environment. Additionally, there is a lack of readily available broadband absorber materials at these frequencies. Furthermore, absorber materials used in chambers and some transverse electromagnetic (TEM) waveguides have limited utility at lower frequencies and often are not well characterized over a wide frequency range. Some previous attempts have been made to use waveguides to determine antenna properties, but they rely on highly approximate methods that only produce qualitative results in certain limits and conditions [8–12]. New methods that are cheaper and easier, without sacrificing accuracy, are highly desirable to further the understanding of both passive and active (nonlinear, time-varying, etc.) antennas [13, 14].

This work presents a new, highly accurate method for determining antenna gain using a transmission-line-based near-field measurement in a waveguide. A mathematical framework for using the S-parameter measurements from a waveguide to calculate antenna gain is presented. Compared to the methods in [8–12], this method provides a highly accurate, direct analytic expression for calculating antenna gain. Additionally, no prior knowledge of the antenna under test (AUT) is required. To validate the proposed method, two monopole antennas are modeled over an infinite ground plane using full-wave electromagnetics. Both are experimentally measured within a waveguide, and it is found that there is very good agreement between the model and measurement. By utilizing a tabletop TEM stripline transmission line waveguide, lower-frequency S-parameter measurements can be easily performed and used to calculate the antenna gain. It is important to note that while the experimental validation provided here is only for electrically small antennas (ESAs), it is anticipated that this method will remain valid in the resonant regime as well, as there are no assumptions made about the AUT presented in the mathematical framework. However, due to the size of self-resonant antennas below 2 GHz, this method is more convenient for ESAs. Large waveguides would be required to accommodate self-resonant antennas at low frequencies; nevertheless, these waveguides would still be smaller and likely cheaper than the anechoic chambers required for equivalent measurements.

2. METHODS

2.1. Theory

Consider the free space Friis equation:

$$P_r(f) = \frac{G_t(f)G_r(f)\lambda_0^2(f)}{16\pi^2 r^2} P_t \tag{1}$$

* Corresponding author: Ryan S. Westafer (Ryan.Westafer@gtri.gatech.edu).

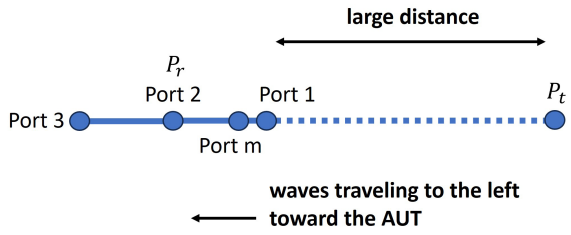

FIGURE 1. Diagram showing the mapping from the free space Friis equation to the waveguide scenario. The waveguide ports are shown connected by solid lines at the left. The hypothetical port, P_t, is shown connected by a dashed line to the right.

In this context, P_r is the received power at the AUT, and P_t is the transmitted power from a known reference antenna. G_t and G_r are the magnitude of the realized antenna gain for the transmitting and receiving antennas, respectively. The term "realized gain" is used in this work to indicate that G, as a power ratio, also includes effects of mismatch and inefficiency. ESAs cannot attain a large directivity, so the mismatch and inefficiency dominate. λ_0 is the wavelength in free space, and r is the distance between the two antennas. Gain itself is a far-field quantity, so r is expected to be many wavelengths in size. Now consider a three-port waveguide measurement with an AUT placed inside the waveguide. In this configuration, there is one port at each end of the waveguide and one port at the AUT. Additionally, consider the case where the AUT is illuminated by a uniform incident field, and the incident wave makes a single pass through the antenna. The latter condition can be achieved by utilizing a well-matched transmission-line-based waveguide and/or time gating techniques. These conditions are analogous to those required for standard antenna measurements in an anechoic chamber. The goal is to mathematically relate the variables in Eq. (1) to the presented waveguide scenario. Fig. 1 shows a diagram relating the two scenarios, where an additional hypothetical port, Port m, has been added and will be discussed later. The term hypothetical is used because this port does not have the termination of any kind (antenna, cable, etc.) However, like any port, it is defined by the fields and impedance over a cross sectional area. The waveguide scenario can be mapped to a free space equivalent by calculating the effective mode area of the incident wave in an empty portion of the main cross section of the waveguide [15, 16]:

$$M_{area}(f) = \frac{\int^{\infty} W(f)dA}{W_0(f)} \tag{2}$$

$$W(f) = \frac{1}{2}\epsilon_0|E(f)|^2 + \frac{1}{2}\mu_0|H(f)|^2 \tag{3}$$

This area of integration is a 2D cross sectional area, as in [15, 16], and the integration extends to infinity. This assumes the material properties inside the waveguide are vacuum (i.e., no dielectric insert). W_0 contains the uniform fields that are incident on the AUT. The effective waveguide mode area is an intrinsic property of the waveguide determined from energy densities and is independent of the AUT. It is expected to remain constant with frequency for a TEM mode, but not for TE or TM modes. For any mode type, this frequency-dependent effective waveguide mode area can be calculated using a full-wave model, or by performing measurements using a known reference antenna. Using a reference antenna is a common practice for antenna measurements in anechoic chambers. The power at Port m can be related to the transmitted power in Eq. (1) by utilizing a well-known near-field to far-field transform approximation within this context [17, 18]:

$$|E_m(f)|^2 \approx \frac{k_0^2(f)}{4\pi^2 r^2}|E_t(f)|^2 M_{area}(f)^2 \tag{4}$$

k_0 is the wave vector in free space, and in this context, the gain of the hypothetical antenna at Port t is given by

$$G_t(f) = \frac{4\pi}{\lambda_0^2(f)} M_{area}(f) \tag{5}$$

This result is less intuitive but can be understood by the fact that the effective aperture area of an antenna is the effective area over which the power is transferred to a plane wave. It is also known that

$$P_r(f) = P_2(f) = |S_{21}(f)|^2 P_1(f) \tag{6}$$

Next, the power at Port m and Port 1 need to be related to one another. At first glance, it might seem odd to create a new, hypothetical port. In real waveguides, there will be a transition from the main cross section of the guide to a feed at the port, often a coaxial cable. This impedance transition will cause some reflections and some loss, though ideally very little to more easily maintain the single pass condition. Thus, while there is not a feed or antenna connected at Port m, it is useful to define a port in this location for the above reasoning. This can be accounted for in this way:

$$P_1(f) = C(f)P_m(f) \tag{7}$$

where $C(f)$ is also an intrinsic property of the waveguide only (i.e., not dependent on the AUT) and will be frequency dependent. It can also be calculated using a full-wave model or by performing measurements of a known reference antenna. Additionally, calibration measurements can be performed to remove this effect. Combining terms:

$$P_r(f) = |S_{21}(f)|^2 C(f) P_m(f) \tag{8}$$

$$\frac{P_r(f)}{P_t} = \frac{|S_{21}(f)|^2 C(f) P_m(f)}{P_t} = \frac{|S_{21}(f)|^2 C(f)|E_m(f)|^2}{|E_t(f)|^2} \tag{9}$$

It was implied, but not directly stated, that the port impedances at Port m and Port t are the same, and the port impedances of Port 1, Port 2, and Port r are the same (typically 50 Ohms). Finally, the magnitude of the realized antenna gain is given by:

$$G_r(f) = \frac{C(f)k_0^2(f)|S_{21}(f)|^2 M_{area}(f)}{\pi} \tag{10}$$

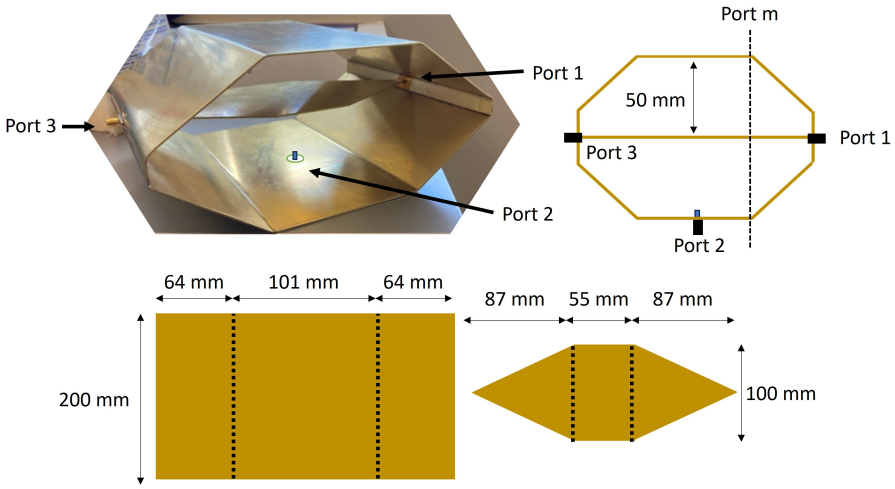

FIGURE 2. Diagram of the three-port stripline waveguide that operates in the TEM mode. A photograph of the real waveguide is shown with an illustration of the coaxial probe (Port 2) used to create the monopole antenna installed in the bottom conducting plane.

A factor of 4 is needed if the infinite ground plane condition is considered due to a doubling of the E-field magnitude:

$$G_r(f) = \frac{4C(f)k_0^2(f)|S_{21}(f)|^2 M_{area}(f)}{\pi} \tag{11}$$

To summarize, the antenna gain can be determined by measuring the transmission coefficient of an AUT using any type of waveguide. All other variables in Eq. (11) are constants that are intrinsic to the waveguide itself or nature, independent of the AUT. It is important to emphasize that no assumptions about the AUT or the type of waveguide have been made. The only requirements are that the incident field be uniform and make a single pass through the AUT. The latter can be achieved using time gating techniques if the waveguide in question is sizable enough to allow for it. However, it can also be done using a highly transmissive waveguide, as is done in this work. Time gating may be problematic if the gate is too narrow relative to the ring-down of the antenna system. For example, an ESA may be brought to resonance and exchange energy with the external field for a considerable time, requiring a larger or more transmissive guide than that might be expected.

2.2. TEM Waveguide

For verification purposes, a stripline waveguide was constructed that operates in the TEM mode from DC up to around 300 MHz, though using a TEM mode is not a requirement. The waveguide and its dimensions are shown in Fig. 2 along with a graphical representation of the coaxial probe used to create the monopole antenna. Two monopole antennas are considered: one with a conductive center pin length of 3 mm and the other with a conductive center pin length near 0 mm. The three-port device was calibrated to remove cable loss and reflections from the S-parameters. $C(f)$ is approximately equal to 1 over this entire frequency range for this highly transmissive waveguide, as seen from Fig. 3, which shows the modeled and measured S-parameters of the stripline waveguide without the installed monopole antenna. An Ansys High Frequency Simulation Software (HFSS) model of the stripline waveguide is also shown in Fig. 3. The effective area of the waveguide mode, using this HFSS model, was calculated to be approximately 0.014 m^2 with some minor variations across the frequency range. This is expected to vary slightly for the actual waveguide. $C(f)$ can also be calculated in HFSS, if desired. Using a reference antenna measurement to calculate the effective area, $C(f)$ would likely be a more accurate approach, but a modeling approach is sufficiently accurate for the purpose of validating the method.

2.3. Monopole Antennas

A full-wave finite-difference time-domain (FDTD) electromagnetics model was used to simulate the gain of a monopole antenna over an infinite ground plane. The FDTD model utilizes Yee's well-known method for solving Maxwell's equations [19–21]. The infinite ground plane condition is emulated by using absorbing boundary conditions near the edges of the simulation. The cell size used here is 0.1 mm such that the important features of the monopole antenna can be accurately captured. The monopole model geometries are shown in Fig. 4. The near 0 mm center pin monopole is modeled with a center pin of 0.2 mm. The real monopole pin protrudes slightly above the ground and is estimated to have a center pin of length 0.2 mm, but this is challenging to measure precisely. A dielectric value of 2.2 is used for the Teflon dielectric insert in the FDTD model, but it is not unusual for Teflon to take on values from 2.0–2.3. Related, the FDTD model port impedance values are closer to 43 Ohms, rather than the supposed 50 Ohms of the real monopoles. This is largely due to the slight differences in real and model coaxial cross sectional areas created by the Yee cell size constraint. The real coaxial connector has an outer diameter of 4.2 mm and an inner pin diameter of 1.3 mm, while the model coaxial connector has an outer diameter of 4.2 mm and an inner pin diameter of 1.4 mm. These collective differences between the modeled antennas and real antennas are expected to minimally impact the comparison. It is important to

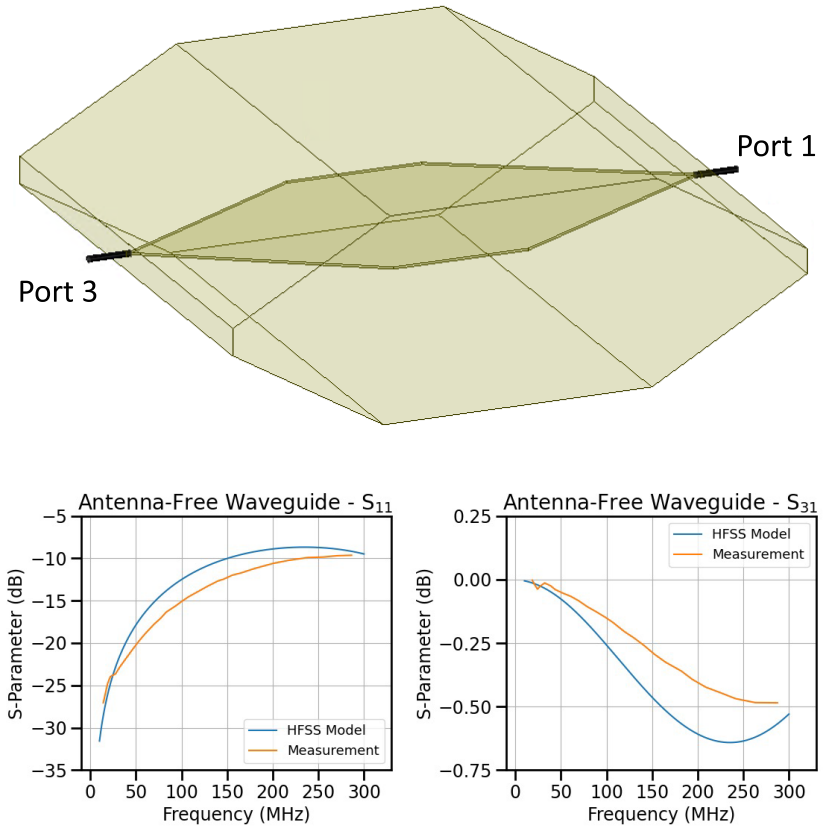

FIGURE 3. Diagram of the HFSS full-wave model of the empty waveguide (i.e., no antenna), along with the modeled and measured S-parameters showing the empty waveguide to be highly transmissive over this frequency range.

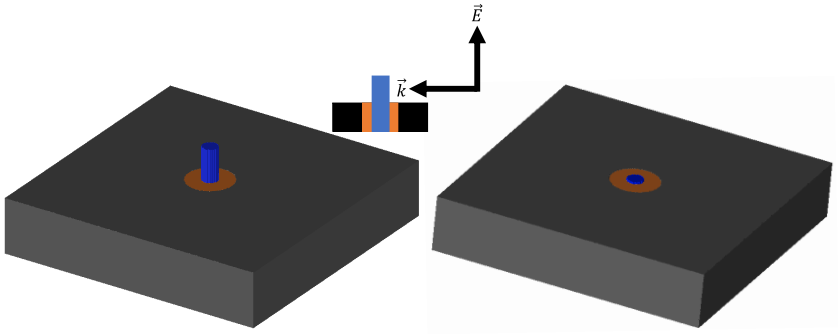

FIGURE 4. FDTD models of the monopole antennas. An infinite ground plane condition is emulated using absorbing boundary conditions at the edges of the ground plane.

highlight that, while both of these antennas are ESAs for convenience of testing, this is not a requirement.

An incident plane wave is excited in the FDTD simulation as illustrated in Fig. 4, representing the mapping condition excited in the waveguide. The gain is only measured in one direction, with only one polarization. This waveguide can be used to obtain angular dependence of the gain as well, if desired. However, these monopole antennas have angular symmetry within the plane. It is also possible to short the waveguide and rotate the AUT orthogonal to the current orientation, but the monopole favors E-fields along the direction shown in Fig. 4, so this is not the preferred scenario. This waveguide is not suitable for looking at additional polarizations, but other waveguides, such as a rectangular waveguide, could be constructed that allow for the excitation of different E-field orientations.

3. RESULTS

The comparison for the gain of the modeled and measured monopole antennas is shown in Fig. 5 from around 10 MHz up to 310 MHz. Overall, there is very good agreement between the modeled and measured cases, adding further validity to the proposed measurement technique. However, though the agreement is very good, there are some differences in the model and measured curves. The dip-like and peak-like features of the

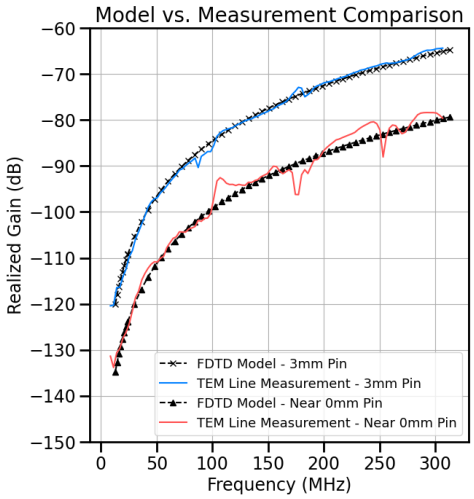

FIGURE 5. Comparison of the gains determined from the FDTD numerical model and the transmission line measurement for both monopole antennas.

measured curves are likely created by calibration errors as there should not be anything highly resonant about the monopole antennas or the waveguide at these frequencies. That is, the realized gain curves are expected to be smooth with no additional features over this frequency range. This is further evident when the 3 mm center pin case is compared to the 0 mm center pin case. It shows similar, yet far weaker responses at the same frequencies, likely indicating calibration error. It should be noted that multiple calibrations were performed, and the peak-like and dip-like responses varied a little each time. Additionally, the near 0 mm center pin case likely extends itself to more calibration error due to the lower overall transmission. The gain of the near 0 mm center pin case is more sensitive to the coaxial cross section and center pin protrusion amount than the 3 mm center pin case, making it more challenging to accurately model than the 3 mm center pin case. Additional differences between the curves can likely be attributed to variations in the real effective waveguide mode area vs. the model determined effective waveguide mode area. Near the higher frequencies, this waveguide begins to support higher order modes. The first non-TEM mode is resonant around 450 MHz in this waveguide. This mode and higher frequency modes are resonant-like, and the waveguide is not long enough to accurately time gate out the response for a single pass, thus placing an upper limit on the frequencies that can be utilized in this particular waveguide. There is likely some small mode mixing near the high end of the frequencies shown in Fig. 3. The lower end of the frequency range will be limited by the capabilities of the analyzer, as there is no cutoff frequency for the TEM waveguide. Recall that the current setup designed for method verification is limited to a single incident, single polarized wave. Future waveguide designs that are longer and would allow time gating are of great interest, in addition to rotating stages to more easily allow for angle-dependent measurements. As stated in the introduction section, it is challenging and burdensome to perform accurate free space measurements at these frequencies for comparison.

4. CONCLUSION

In conclusion, this paper presents a new, highly accurate method for determining antenna gain. This near-field transmission line based method for determining antenna gain accommodates ESAs more easily, but the technique is not restricted to ESAs only. Additionally, while this method is attractive for measurements at low frequencies, it is also valid at high frequencies as well. This table-top method will likely enable faster, cheaper, and easier low frequency antenna characterization, while maintaining or improving accuracy. Future studies that further validate this new method under more conditions are of great interest.

ACKNOWLEDGEMENT

This research was developed with funding from the Defense Advanced Research Projects Agency (DARPA). The views, opinions and/or findings expressed are those of the author and should not be interpreted as representing the official views or policies of the Department of Defense or the U.S. Government. The authors would like to thank John Burke, Ben Epstein, and Jonathan Hoffman of the DARPA Microsystems Technology Office (MTO). Distribution Statement A — Approved for Public Release, Distribution Unlimited.

REFERENCES

[1] IEEE, "IEEE standard for definitions of terms for antennas," *IEEE Std 145-2013 (Revision of IEEE Std 145-1993)*, 1–50, 2014.

[2] IEEE, "IEEE recommended practice for antenna measurements," *IEEE Std 149-2021 (Revision of IEEE Std 149-1977)*, 1–207, 2022.

[3] Nahman, N. S., M. Kanda, E. B. Larsen, and M. L. Crawford, "Methodology for standard electromagnetic field measurements," *IEEE Transactions on Instrumentation and Measurement*, Vol. 34, No. 4, 490–503, 1985.

[4] Zheng, Y., B. Lin, T. H. Loh, and Y. Qi, "A novel gain reference dipole antenna for accurate calibration of over-the-air measurement systems," *IEEE Transactions on Instrumentation and Measurement*, Vol. 72, 1–10, 2023.

[5] Blech, M. D., M. M. Leibfritz, R. Hellinger, D. Geier, F. A. Maier, A. M. Pietsch, and T. F. Eibert, "Time-domain spherical near-field antenna measurement system employing a switched continuous-wave hardware gating technique," *IEEE Transactions on Instrumentation and Measurement*, Vol. 59, No. 2, 387–395, 2010.

[6] Balanis, C. A., *Antenna Theory: Analysis and Design*, 4th ed., John Wiley & Sons, New York, 2016.

[7] Pozar, D. M., *Microwave Engineering*, 3rd ed., Wiley, Hoboken, NJ, 2005.

[8] Morioka, T., "Response of a short-dipole probe to a nonuniform E-field of a TEM cell," *IEEE Transactions on Instrumentation and Measurement*, Vol. 60, No. 7, 2709–2714, 2011.

[9] Koohestani, M., M. Ramdani, F. Lafon, A. A. Moreira, and R. Perdriau, "Impact of field polarization on radiated emission characterization in an open TEM cell," *IEEE Transactions on Instrumentation and Measurement*, Vol. 69, No. 9, 6595–6602, 2020.

[10] Wilson, P. F., "Antenna gain-factor equivalent for TEM cells," in *IEEE International Symposium on EMC*, Einhoven, NL, Sep.

2004.

[11] Ji, R., F. Zhou, X. Yuan, and K. Cheng, "A novel method to measure small antennas using a wideband coaxial cone TEM cell," *Microwave and Optical Technology Letters*, Vol. 65, No. 12, 3269–3274, Dec. 2023.

[12] Kaverine, E., S. Palud, F. Colombel, and M. Himdi, "Simple approach to miniaturized antenna gain measurement using a parallel plate cell in the HF band," *Progress In Electromagnetics Research M*, Vol. 46, 11–18, 2016.

[13] Strachen, N., J. H. Booske, and N. Behdad, "Class-E, active electrically small antenna with enhanced bandwidth-efficiency product and high radiated power at the high-frequency (HF) band," *Journal of Applied Physics*, Vol. 135, No. 22, 224502, 2024.

[14] Backes, K. M., P. K. Elgee, K.-J. LeBlanc, C. T. Fancher, D. H. Meyer, P. D. Kunz, N. Malvania, K. L. Nicolich, J. C. Hill, *et al.*, "Performance of antenna-based and Rydberg quantum RF sensors in the electrically small regime," *Applied Physics Letters*, Vol. 125, No. 14, 144002, 2024.

[15] Zhou, Y., Y. Wang, K. Yvind, N. Gregersen, and M. Pu, "Ultra-small mode area V-groove waveguide design for on-chip single-photon emission," *Optics Express*, Vol. 32, No. 2, 2884–2893, Jan. 2024.

[16] Gui, C. and J. Wang, "Wedge hybrid plasmonic THz waveguide with long propagation length and ultra-small deep-subwavelength mode area," *Scientific Reports*, Vol. 5, No. 1, 11457, Jul. 2015.

[17] Stephanson, M., "A fast near- to far-field transform algorithm," Ph.D. dissertation, Ohio State University, Columbus, OH, USA, 2007.

[18] Jackson, J. D., *Classical Electrodynamics*, 3rd ed., Wiley, New York, NY, 1999.

[19] Yee, K., "Numerical solution of initial boundary value problems involving Maxwell's equations in isotropic media," *IEEE Transactions on Antennas and Propagation*, Vol. 14, No. 3, 302–307, 1966.

[20] Sullivan, D. M., *Three-dimensional Simulation*, 79–108, Wiley-IEEE Press, 2000.

[21] Taflove, A. and S. C. Hagness, *Computational Electromagnetics: The Finite-Difference Time-Domain Method*, 3rd ed., Artech House, Norwood, 2005.